New Mexico Geological Society

Downloaded from: https://nmgs.nmt.edu/publications/guidebooks/45



The Horse Springs Dacite--An enigmatic pyroclastic deposit at the edge of the Plains of San Agustin

James C. Ratte, Peter J. Modreski, William C. McIntosh, and Richard M. Chamberlin
1994, pp. 193-207. https://doi.org/10.56577/FFC-45.193

in:

Mogollon Slope (West-Central New Mexico and East-Central Arizona), Chamberlin, R. M.; Kues, B. S.; Cather, S. M.; Barker, J. M.; McIntosh, W. C.; [eds.], New Mexico Geological Society 45th Annual Fall Field Conference Guidebook, 335 p. https://doi.org/10.56577/FFC-45

This is one of many related papers that were included in the 1994 NMGS Fall Field Conference Guidebook.

Annual NMGS Fall Field Conference Guidebooks

Every fall since 1950, the New Mexico Geological Society (NMGS) has held an annual Fall Field Conference that explores some region of New Mexico (or surrounding states). Always well attended, these conferences provide a guidebook to participants. Besides detailed road logs, the guidebooks contain many well written, edited, and peer-reviewed geoscience papers. These books have set the national standard for geologic guidebooks and are an essential geologic reference for anyone working in or around New Mexico.

Free Downloads

NMGS has decided to make peer-reviewed papers from our Fall Field Conference guidebooks available for free download. This is in keeping with our mission of promoting interest, research, and cooperation regarding geology in New Mexico. However, guidebook sales represent a significant proportion of our operating budget. Therefore, only *research papers* are available for download. *Road logs*, *mini-papers*, and other selected content are available only in print for recent guidebooks.

Copyright Information

Publications of the New Mexico Geological Society, printed and electronic, are protected by the copyright laws of the United States. No material from the NMGS website, or printed and electronic publications, may be reprinted or redistributed without NMGS permission. Contact us for permission to reprint portions of any of our publications.

One printed copy of any materials from the NMGS website or our print and electronic publications may be made for individual use without our permission. Teachers and students may make unlimited copies for educational use. Any other use of these materials requires explicit permission.

This page is intentionally left blank to maintain order of facing pages.

New Mexico Geological Society

Downloaded from: http://nmgs.nmt.edu/publications/guidebooks/45



The Horse Springs Dacite--An enigmatic pyroclastic deposit at the edge of the Plains of San Agustin

James C. Ratte, Peter J. Modreski, William C. McIntosh, and Richard M. Chamberlin, 1994, pp. 193-207

in:

Mogollon Slope (West-Central New Mexico and East-Central Arizona), Chamberlin, R. M.; Kues, B. S.; Cather, S. M.; Barker, J. M.; McIntosh, W. C.; [eds.], New Mexico Geological Society 45th Annual Fall Field Conference Guidebook, 335 p.

This is one of many related papers that were included in the 1994 NMGS Fall Field Conference Guidebook.

Annual NMGS Fall Field Conference Guidebooks

Every fall since 1950, the New Mexico Geological Society (NMGS) has held an annual Fall Field Conference that explores some region of New Mexico (or surrounding states). Always well attended, these conferences provide a guidebook to participants. Besides detailed road logs, the guidebooks contain many well written, edited, and peer-reviewed geoscience papers. These books have set the national standard for geologic guidebooks and are an essential geologic reference for anyone working in or around New Mexico.

Free Downloads

NMGS has decided to make peer-reviewed papers from our Fall Field Conference guidebooks available for free download. Non-members will have access to guidebook papers two years after publication. Members have access to all papers. This is in keeping with our mission of promoting interest, research, and cooperation regarding geology in New Mexico. However, guidebook sales represent a significant proportion of our operating budget. Therefore, only *research papers* are available for download. *Road logs*, *mini-papers*, *maps*, *stratigraphic charts*, and other selected content are available only in the printed guidebooks.

Copyright Information

Publications of the New Mexico Geological Society, printed and electronic, are protected by the copyright laws of the United States. No material from the NMGS website, or printed and electronic publications, may be reprinted or redistributed without NMGS permission. Contact us for permission to reprint portions of any of our publications.

One printed copy of any materials from the NMGS website or our print and electronic publications may be made for individual use without our permission. Teachers and students may make unlimited copies for educational use. Any other use of these materials requires explicit permission.

This page is intentionally left blank to maintain order of facing pages.

THE HORSE SPRINGS DACITE—AN ENIGMATIC PYROCLASTIC DEPOSIT AT THE EDGE OF THE PLAINS OF SAN AGUSTIN

JAMES C. RATTÉ[1], PETER J. MODRESKI[1],
WILLIAM C. MCINTOSH[2], and RICHARD CHAMBERLIN[2]
[1]U.S. Geological Survey, Denver, CO 80225; [2]New Mexico Bureau of Mines and Mineral Resources, Socorro, NM 87801

Abstract—The Horse Springs dacite (new, but informal, name) is a local pyroclastic deposit near the southwest end of the Plains of San Agustin and the settlement of Old Horse Springs. The regional Blue Canyon Tuff (Eocene) underlies the Horse Springs dacite, is indistinguishable from it in age (~33.7 Ma), and is petrographically and chemically similar to the dacite; the enigma is the relationship, if any, of these two units. These similarities and the distribution of the Blue Canyon Tuff, which has no known source, suggest the possibility of a genetic relationship and a possible caldera source for both formations beneath the Plains of San Agustin. The Horse Springs dacite consists of pumice flows and block-and-ash flows at least 250 m thick. Outcrops of the dacite near the edge of the plains, closest to the suspected source, contain juvenile, pumiceous dacite blocks, 2-3 m long, and cognate quartz monzonite blocks of the same size. The dacite also contains accidental inclusions of mineralized jasperoid as large as 0.5 m across, derived from pre-Tertiary sedimentary rocks, including limestone, sandstone, and calcareous argillaceous rocks. The jasperoid inclusions, where found in place, have calc-silicate, skarn-type reaction rims consisting of diopside, rare garnet, and seemingly incompatible clay minerals. Many inclusions also have iron- and zinc-enriched cores that contain as much as 1% zinc, mainly in magnesioferrite. Both the cognate quartz monzonite inclusions and the accidental mineralized jasperoid inclusions are interpreted as having been stoped from the roof of the dacite magma chamber prior to eruption. The skarn reaction rims, however, are believed to have formed after eruption, during the cooling of the enclosing block-and-ash flows, which is indicated by the delicate, granular and friable nature of the rims, the presence of clay minerals, and the absence of unaltered limestone inclusions within the dacite.

INTRODUCTION

The Horse Springs dacite is a near-vent, pyroclastic deposit that is represented by a narrow, north-south outcrop belt about 5 km wide and 20 km long, on the north side of the San Agustin plains near Old Horse Springs (Figs. 1, 2). The enigma is related to its petrographic and chemical resemblance to the Blue Canyon Tuff (Eocene), and its possible significance to a caldera source for the Blue Canyon Tuff and (or) other ignimbrites in the upper part of the Eocene to early Oligocene Datil Group, and the origin and significance of the abundant inclusions of quartz monzonite and mineralized pre-Tertiary rocks which it contains.

Here we recognize the Horse Springs dacite as an informal volcanic stratigraphic unit and update a previous discussion of its age, origin and unique inclusions (Ratté and Modreski, 1989). The Horse Springs dacite was first described as the middle tuff-breccia sequence, at least 150 m thick, of the lower rhyolite pyroclastic unit of the Datil Formation (Stearns, 1962, p. 14-16), which he considered to have been "erupted from a center at no great distance." Later, Bornhorst (1976) and Jones (1980) called these rocks the tuff breccia of Horse Springs Canyon and gave the first detailed description of their petrography, composition, distribution and approximate age. Bornhorst and Elston (1978) and Elston (1984) correlated the eruption of these tuff breccias to the ring-fracture of the proposed Crosby Mountains cauldron. On the geologic map of the Horse Springs West quadrangle (Ratté et al., 1991), these rocks were called the pumice breccia of Old Horse Springs to bring the name into conformance with the most recent geo-

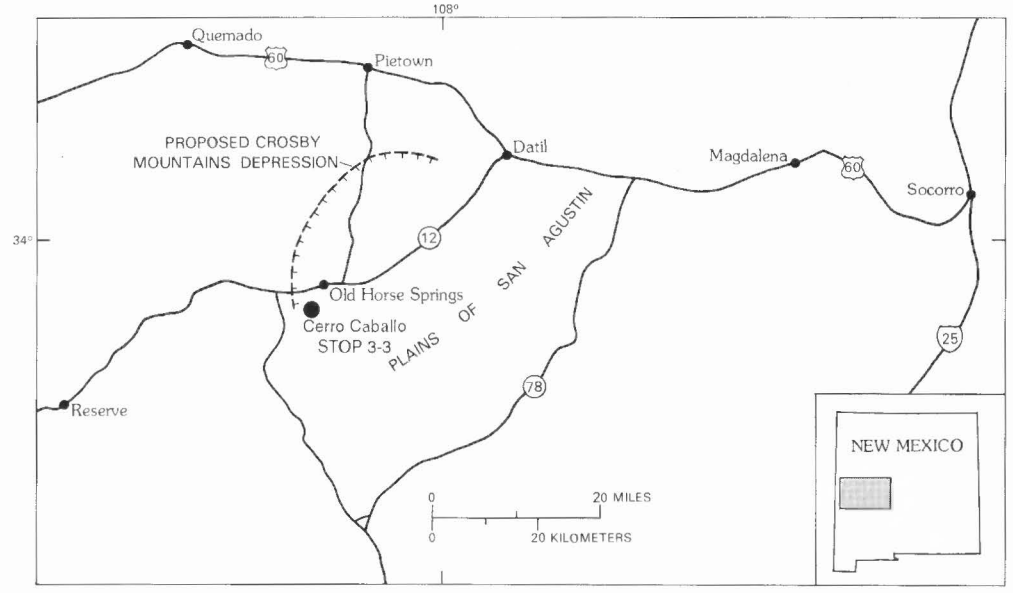


FIGURE 1. Index map showing location of Horse Springs dacite vent facies at Cerro Caballo, southwest of Old Horse Springs. Outline of Crosby Mountains depression is shown here as proposed by Bornhorst (1976) and Elston (1984).

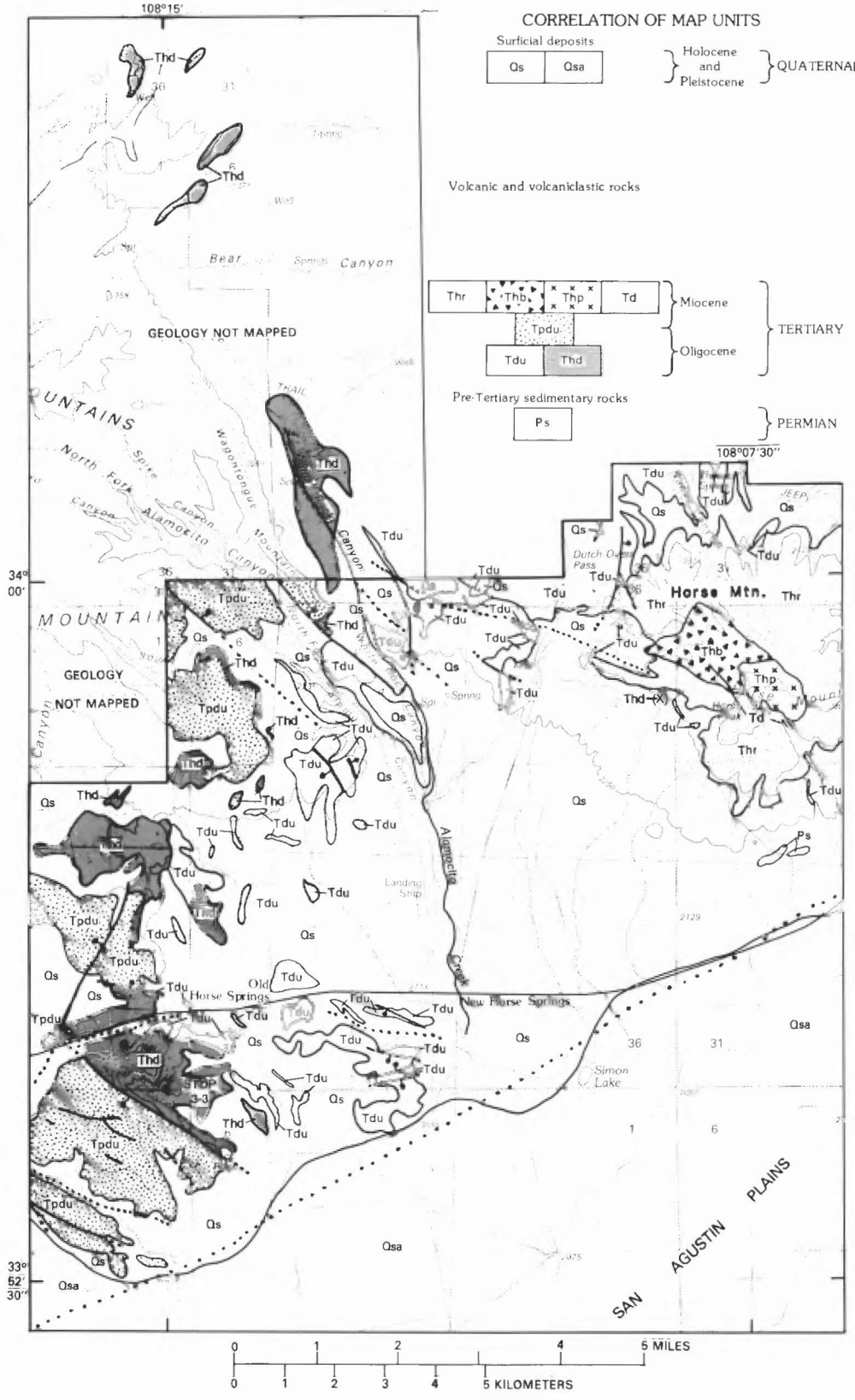


FIGURE 2. Geologic map showing distribution of Horse Springs dacite, Thd (solid black). Modified from Ratté et al., (1988, pl. 1) and Jones (1980, fig. 1). Qs = Surficial deposits, undivided (Holocene and Pleistocene); Qsa = fluviolacustrine deposits of Lake San Agustin (Holocene and Pleistocene); Rocks of the Horse Mountain volcano (Miocene, about 13 Ma): Thr = dacite and rhyolite lava flows; Thb = dacite and rhyolite domal vent breccias; Thp = rhyolite plug; Td= rhyolite dikes; Tpdu, = post-Datil Group volcanic and volcaniclastic rocks, undivided (Miocene? and Oligocene); Tdu = volcanic and volcaniclastic rocks of Datil Group, undivided (Oligocene); Ps = Permian sedimentary rocks, undivided.

graphic names in the area. However, here we propose that these rocks be called Horse Springs dacite to emphasize the composition of the rocks and in anticipation that the springs at Old Horse Springs may well outlive the historic settlements that were named for them.

STRATIGRAPHY AND LITHOLOGY

The known distribution of the Horse Springs dacite is confined to the Horse Mountain West, Bell Peak, Wallace Mesa and Mangas Mountains 7 1/2-minute quadrangles. The outcrops are mostly west of White Rock and Alamocito canyons, but one tiny outcrop on the west flank of Horse Mountain (shown by an x on Fig. 2) indicates that the dacite probably once covered a much larger area, but it is now buried by younger rocks or has been downfaulted beneath the Plains of San Agustin. These pyroclastic rocks have a maximum thickness of about 250 m southwest of Old Horse Springs on the ridge that on earlier maps (USGS 30-minute Pelona quadrangle) is called Cerro Caballo (Fig. 1), and is the site for Stop 3, Day 3 of the Field Trip described in the front section of this Guidebook. The pyroclastic deposit thins northward and is less than 30 m thick where last observed in the Wallace Mesa and Mangas Mountains quadrangles (Jones, 1980).

The Horse Springs dacite underlies Hells Mesa Tuff (32 Ma) in the northwestern part of the Horse Springs West quadrangle (Ratté et al., 1991) and thus is in the upper part of the Datil Group of Osburn and Chapin (1983), Cather (1986) and Cather et al. (1987). The dacite unconformably overlies ash-flow tuffs of the Datil Group, including Blue Canyon Tuff (33.7 Ma) and Rock House Canyon Tuff (34.4 Ma) and intertongued volcaniclastic sedimentary rocks of the Spears Group (Cather et al., this volume). Two new $^{40}Ar/^{39}Ar$ ages (sanidine laser-fusion ages, from cognate quartz monzonite blocks and pumice blocks included in the dacite) have an average age of 33.73 Ma (Table 1), virtually identical to the age of the underlying Blue Canyon Tuff. Previously reported ages for the dacite and its included quartz monzonite blocks, which ranged from about 35.5 Ma to about 31.2 Ma, are summarized by Marvin et al. (1987).

The Horse Springs dacite comprises three main lithologic facies, a basal breccia, lower pumice breccia flows with a mantle of ash-cloud surge beds, and upper block-and-ash flows.

The basal breccia, which ranges from mesobreccia to megabreccia, has been observed only locally, but it is present at the south end of the outcrop belt and may extend to the outcrops at the south end of Wagontongue Mountain (Fig. 2). The mesobreccia contains blocks of Rock House Canyon Tuff and Blue Canyon Tuff, as much as 5 m long, and smaller blocks of fine-grained red andesite and round pebble conglomerate like that in the Spears Group, all in a matrix of Horse Springs dacite. Megabreccia outcrops may actually be layers of mixed Rock House Canyon and Blue Canyon mesobreccia blocks, but some outcrops near the southern end of the Horse Springs dacite outcrop belt seem to be homogeneous slabs of tuff tens of meters long. Approximately the lower half of the Horse Springs dacite pyroclastic deposit, on the Cerro Caballo ridge southwest of Old Horse Springs, consists mainly of coarse, pumice-breccia flows. These are best exposed on the slickrock slope on the eastern side of the ridge where flows 1 and 2 (Fig. 3) are separated by a parting that probably represents a change in the size of pumice clasts produced by a pulsating eruption column. Both flow units show reverse size-grading of pumice blocks (Figs. 4, 5). The pumice flows were probably once mantled widely by surge deposits, which now are preserved erratically along the base of the cliffs at the top of the pumice flows (Fig. 6). The crossbedded deposits are probably best described as ash-cloud surge deposits (Fisher and Schminke, 1984, p. 201, 219).

Approximately the upper half of the Horse Springs dacite on the ridge southwest of Old Horse Springs is probably best described as a block-and-ash flow deposit, which may have been produced by "boiling over without a vertical eruption column" (Fisher and Schminke, 1984, p. 189). This facies of the deposit begins above the surge deposit at the base of the sharp cliff, above the lower pumice flows, and is remarkable in several respects. The 10-20-m-high fluted cliffs at the base of the block-and-ash flows display an ancient fumarole zone (Figs. 3, 7) that consists of numerous degassing pipes in which the fine-grained constituents of the flows are depleted by elutriation. The pipes here lack any evidence of mineralization accompanying the degassing and are unusual in being at the bottom of the deposit rather than at the top (Smith, 1960; Fisher and Schminke, 1984, particularly fig. 8-21).

The block-and-ash flows contain large blocks of pumiceous dacite (Fig. 8) and cognate inclusions of coarsely porphyritic quartz monzonite, commonly 2-3 m long (Fig. 9), in a somewhat finer matrix of dacite breccia. Quartz monzonite inclusions are present in all three facies of the Horse Springs dacite, but large blocks are most concentrated near the base of the block-and-ash flows, particularly on the ridge southwest of Old Horse Springs. Blocks of pumiceous dacite, having dimensions of approximately 1 m, are present in the block-and-ash flows all the way to White Rock Canyon. However, quartz monzonite inclusions in outcrops other than those on the ridge southwest of Old Horse Springs are generally ash- or lapilli-sized fragments.

TABLE 1. $^{40}Ar/^{39}Ar$ laser-fusion data for Horse Springs dacite. Each analysis is one laser fusion of a collection of 5 to 20 crystals, analyzed at the New Mexico Geochronology Research Laboratory. Ages are relative to Fish Canyon Tuff sanidine (27.84 Ma). Italicized data not used in calculation of mean age. Measured discrimination=1.0081. Correction factors: $^{39}Ar/^{37}ArCa$=0.0007, $^{36}Ar/^{37}ArCa$=0.00027, $^{40}Ar/^{39}ArK$=0.0225. Decay constants after Steiger and Jaeger (1977).

L#	40/39	37/39	36/39	39K moles	K/Ca	%40*	Age	±Err
Sample OSHBX-1, pumice block, sanidine, J + 0.004019 ± 0.00001								
292-01A	4.73	1.27E-02	1.37E-05	2.2E-16	40.2	99.5	33.763	0.072
292-04A	4.73	1.39E-02	2.79E-05	2.9E-16	36.6	99.4	33.789	0.066
292-05A	4.74	1.47E-02	2.88E-05	2.8E-16	34.8	99.4	33.806	0.070
292-07A	4.74	1.24E-02	2.43E-05	1.1E-16	41.2	99.4	33.826	0.071
292-06A	4.74	1.22E-02	8.30E-06	3.4E-16	41.9	99.5	33.857	0.063
292-08A	4.74	1.38E-02	2.74E-05	3.2E-16	37.0	99.4	33.861	0.072
292-03A	4.74	1.21E-02	2.47E-05	2.3E-16	42.2	99.4	33.865	0.066
292-02A	4.76	1.27E-02	2.89E-05	2.0E-16	40.1	99.4	33.939	0.072
					mean	**n=8**	33.838	0.055
Sample OSHBX-2, quartz monzonite, sanidine and plagioclase, J = 0.004019 ±0.00001								
293-03A	4.72	3.86E-02	9.24E-05	1.4E-16	13.2	99.0	33.572	0.071
293-06A	4.77	4.63E-02	2.47E-04	1.6E-16	11.0	98.1	33.576	0.073
293-04A	4.75	6.10E-02	1.81E-04	9.2E-17	8.4	98.5	33.627	0.076
293-01A	4.75	3.47E-02	1.55E-04	2.3E-16	14.7	98.6	33.636	0.072
293-05A	4.76	3.74E-02	1.09E-04	1.3E-16	13.6	98.9	33.768	0.071
293-02A	5.02	3.29E-02	1.99E-04	1.6E-16	15.5	98.4	*35.474*	0.077
					mean	**n=5**	33.636	0.080



FIGURE 3. Horse Springs dacite on east-facing slopes of Cerro Caballo ridge southwest of Old Horse Springs. Numbers 1-6 indicate the following: 1 and 2 = non-welded pumice flows, each on the order of 50 m thick; 3 = position of discontinuous, crossbedded, ash-cloud, surge deposits at top of pumice flow no. 2; 4 = ancient fumarole zone in cliffs at base of block-and-ash deposit; 5 = approximate position of parting ledge within zone where 2-3 m blocks of pumiceous dacite and cognate quartz monzonite are concentrated; 6 = approximate top of zone in which mineralized jasperoid inclusions are most concentrated.

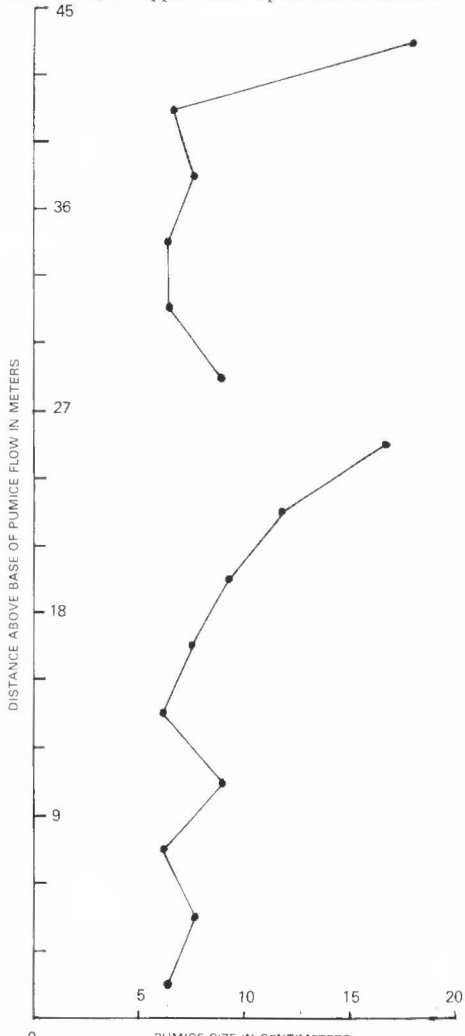


FIGURE 4. Average dimensions of pumice blocks and lapilli in 3-m intervals plotted against position above base of pumice flow no. 2 in Fig. 3. Pumice measured in plane of foliation perpendicular to a tape stretched across the outcrop.



FIGURE 5. Pumice flow no. 2, in Fig. 3, beneath fluted cliffs with ancient fumaroles. Tape stretched across outcrops was used to measure size of pumice pyroclasts, which show reverse grading.



FIGURE 6. Ash-cloud surge beds preserved locally at the top of the pumice flows in the lower part of the Horse Springs dacite, on the east side of the Cerro Caballo ridge southwest of Old Horse Springs.

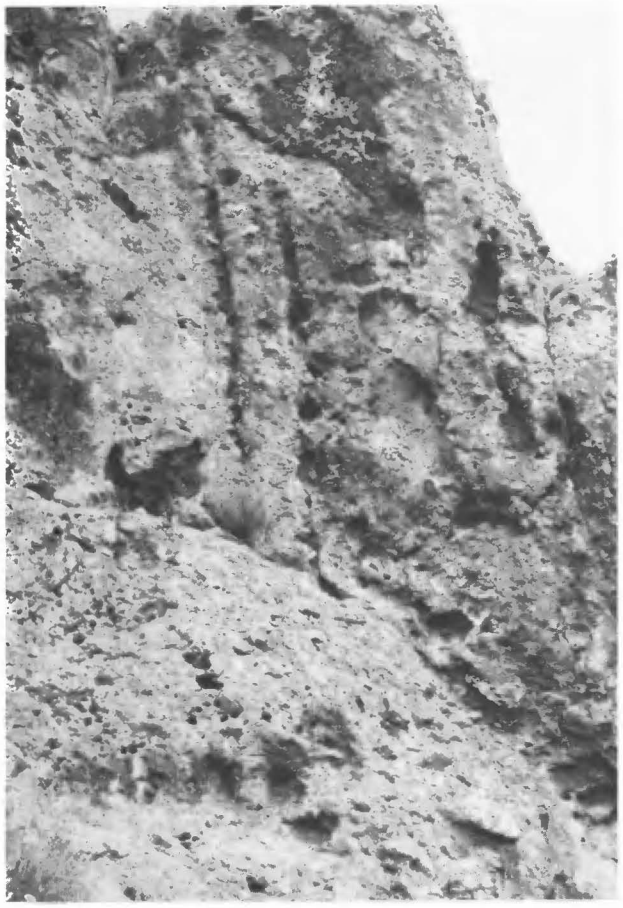


FIGURE 7. Ancient fumarole degassing pipes at the base of the block-and-ash flows in the upper part of the Horse Springs dacite, on the east side of Cerro Caballo ridge southwest of Old Horse Springs (Fig. 3). Width of outcrop is about 3 m.



FIGURE 8. Meter size block of juvenile pumiceous dacite in Horse Springs dacite on west side of Cerro Caballo ridge southwest of Old Horse Springs.

Also distributed throughout the block-and-ash flows, but found in outcrop mainly on the ridge southwest of Old Horse Springs, are unique inclusions of mineralized jasperoid derived from the alteration of pre-Tertiary basement rocks. These xenoliths are sparsely concentrated above a parting ledge (no. 5 on Fig. 3), about 30 m above the base of the block-and-ash flows, and are apparently most abundant between points 5 and 6 on the photo. The zone containing jasperoidized xenoliths also appears to coincide with the upper part of the



FIGURE 9. One to two meter diameter blocks of cognate quartz monzonite and juvenile pumiceous dacite on the east side of Cerro Caballo ridge, at the level of the main concentration of jasperoid blocks, point 5 in Fig. 3.

zone of greatest concentration and maximum size of cognate quartz monzonite blocks; this observation may be significant in interpreting the origin of the jasperoid. Protoliths for the jasperoidized xenoliths can probably be found in the Lower Permian sequence of the Yeso Formation (mainly calcareous to argillaceous sandstone), Glorieta Sandstone and San Andres Limestone, all of which are exposed nearby in outcrops at the foot of Horse Mountain, 12-15 km east of the Cerro Caballo ridge. The largest pre-Tertiary xenolith observed by us was a brick-red block of jasperoidized limestone (Fig. 10) about 50x15x15cm. That the majority of the jasperoid xenoliths have a limestone protolith is indicated by the presence of relict chert nodules (Fig. 11). Jasperoidized limestone inclusions generally have reaction borders composed of calc-silicate skarn a few centimeters thick (Fig. 12), which consist mainly of diopside and clay minerals, with or without garnet and phlogopite. Similar reaction rims border xenoliths that were formerly calcareous and argillaceous sandstones, but are absent on inclusions that are believed to have been sandstone or quartzite.

PETROGRAPHY AND CHEMISTRY OF THE HORSE SPRINGS DACITE

The Horse Springs dacite is a pinkish-brown, pumiceous, fine-grained, granular rock that contains between 25 and 35% 1-4 mm long phenocrysts. The phenocrysts are mainly sodic plagioclase (oligoclase-andesine) about 20-25%, subequal amounts of biotite and clinopyroxene totaling 5-10%, opaque oxides averaging about 7%, and traces of quartz, zircon and apatite. The matrix is a subvitreous, fine-grained spherulitic to granular intergrowth of feldspar and quartz that contains abundant equant to rounded crystals of quartz, plagioclase, and alkali feldspar having dimensions of about 0.1-0.3 mm that give the matrix a sieve-like texture (Fig. 13A, B). The potassic feldspar can be recognized from carlsbad twinned crystals, low refractive index, and by staining.

The quartz monzonite inclusions have a much coarser porphyritic texture than the enclosing dacite, containing abundant plagioclase phenocrysts 1-2 cm long, and having a total phenocryst content of about 40%. Otherwise, the quartz monzonite is quite similar mineralogically and chemically to the dacite (Table 2), differing mainly in having trace amounts of sanidine phenocrysts to about 1 mm long, trace amounts of brown hornblende microphenocrysts, and aphanitic groundmass that ranges from slightly devitrified brown glass to a granophyric matrix of quartz and alkali feldspar with an average grain size of about 0.1 mm. Where the matrix is not granophyric, it has the same sieve texture of rounded to equant small quartz and feldspar crystals scattered through the subvitreous groundmass as the enclosing dacite (Fig. 14). The textural and compositional similarities between the dacite and the quartz monzonite inclusions suggest that the inclusions were derived from an earlier stage of crystallization of



FIGURE 10. Accidental inclusion of jasperoidized limestone from block-and-ash flows in upper part of Horse Springs dacite on east side of Cerro Caballo ridge southwest of Old Horse Springs. Relict bedding is visible.



FIGURE 11. Accidental inclusion of jasperoidized limestone showing relict chert nodules.

the same magma that erupted to form the dacite pumice flows and block-and-ash flows.

The size and abundance of 2-3 m blocks of pumiceous dacite and cognate quartz monzonite inclusions in the Horse Springs dacite at Cerro Caballo, southwest of Old Horse Springs, indicate close proximity to an eruptive vent for the Horse Springs dacite. Further support for the location of a vent in this area is given by the concentration of degassing pipes, ash-cloud surge deposits, the presence of mesobreccia and possibly megabreccia of older rocks, and the thinning and decreased particle size of the deposits northward, away from this area, which is the only direction in which substantial outcrops of the dacite are preserved at the surface. However, there are no vent structures, such as major crossbedded or crosscutting deposits, to indicate that the dacite at Cerro Caballo is within or above the actual conduit, which is most likely buried nearby beneath the alluvium on the Plains of San Agustin.

BLUE CANYON TUFF

The petrography and composition of the Blue Canyon Tuff and the Horse Springs dacite (Table 2) are similar but not identical. The Blue Canyon Tuff could be a slightly more evolved, early eruptive facies of the same magma that produced the Horse Springs dacite. The Blue Canyon Tuff is a low-silica rhyolite (Table 2); it contains between 15-25% phenocrysts, and it differs from Horse Springs dacite mainly in containing more abundant sanidine phenocrysts relative to plagioclase (about 1:2) and a lower abundance of clinopyroxene. Eutaxitic pumice lapilli are obvious in most outcrops, and the matrix of the Blue Canyon Tuff has a vitroclastic texture of devitrified glass shards (Fig. 15) which clearly identifies its ignimbrite origin.

No source is known for the Blue Canyon Tuff, but its regional distribution from the Horse Springs area to the Socorro area indicates that it probably is a caldera-derived ash-flow tuff. At present, the only clues to its source are its distribution and thickness. Blue Canyon Tuff directly underlies the Horse Springs dacite on the east side of the Cerro Caballo ridge southwest of Old Horse Springs, where its 10-15 m thickness is similar to that elsewhere in the Horse Mountain quadrangle (Ratté et al., 1991) and the Horse Springs area. Its maximum thickness in the Datil Mountains (north of Datil) is only about 30 m (Osburn and Chapin, 1983); from the Datil Mountains, the Blue Canyon Tuff thins eastward and is present only locally in the Magdalena-Socorro area. Thus, nowhere is a thickness of Blue Canyon Tuff sufficient to suggest an intracaldera sequence in its known area of distribution, unless it is buried beneath a down-faulted basin such as the Plains of San Agustin. Because of their petrographic similarity and identical isotopic ages, it is plausible that the sources of the Blue Canyon Tuff and the Horse Springs dacite are related, and that both are hidden somewhere beneath the plains in the vicinity of Old Horse Springs (Fig. 1).

PETROGRAPHY AND CHEMISTRY OF MINERALIZED XENOLITHS

The jasperoid inclusions vary in mineral composition from nearly pure quartz, to quartz plus abundant calcite and iron oxides, to dominantly iron oxides. Many inclusions have a concentrically banded core of layers rich in quartz and iron oxides surrounded by brick-red, massive, spherulitic jasperoid (Fig. 16A). Most of the analyzed nodules were collected from float and probably represent the cores of larger jasperoid blocks (Fig. 16B-D); others, which show relict bedding, may have been originally sandstone or quartzite rather than limestone. Most of the quartz in the xenoliths exhibits fibrous or radiating (spherulitic) crystallization, indicating an origin by replacement or recrystallization (Fig. 17), but some show the relict clastic texture of the original sandstone or siltstone.

Iron in the xenoliths forms an unusual suite of ferric-iron minerals, including coarsely crystalline, black, lustrous plates of hematite and red, very fine-grained crystals of magnesioferrite ($MgFe^{3+}2O4$), which are disseminated in the silica and concentrated along quartz grain boundaries. The jasperoid nodules typically have brick-red, fine-

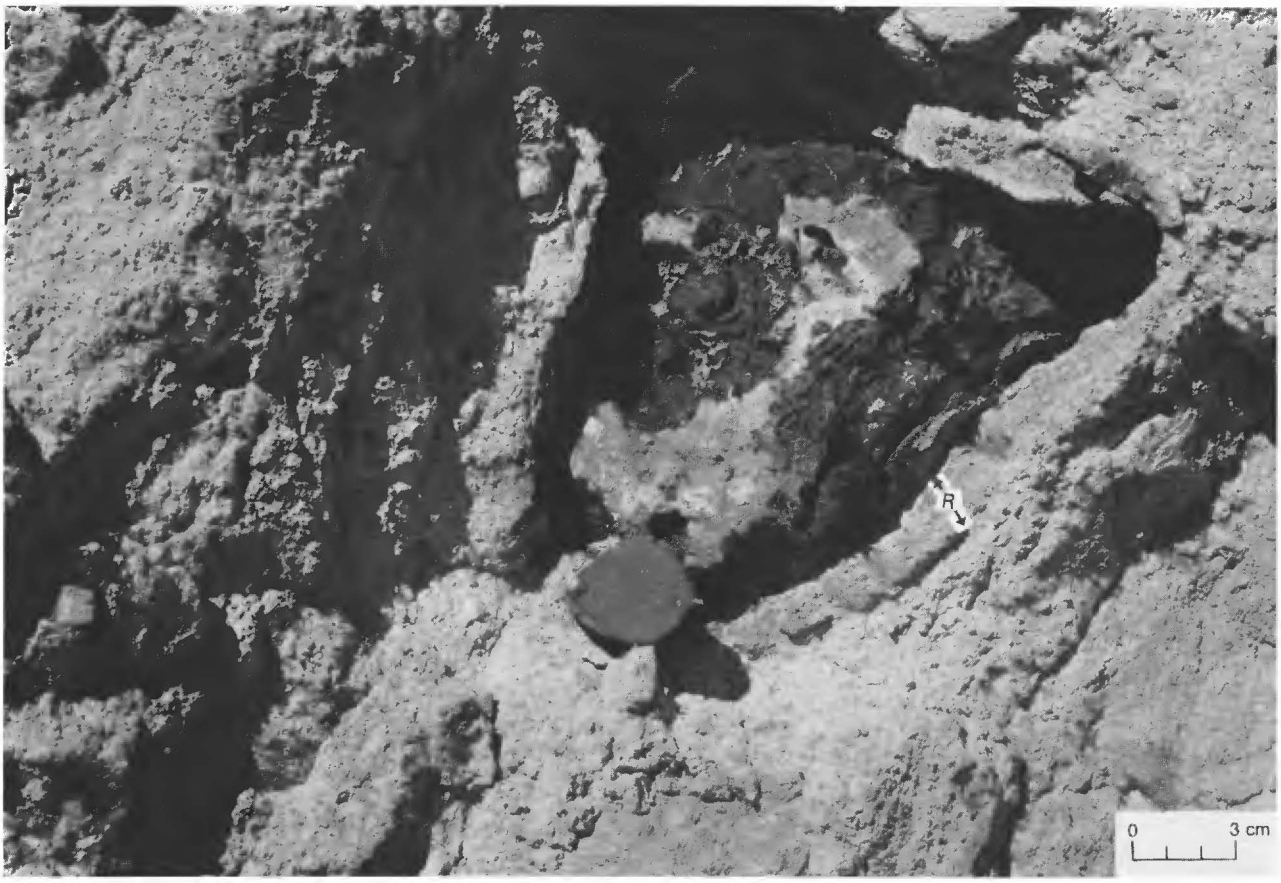


FIGURE 12. Accidental jasperoidized and mineralized inclusion in situ in Horse Springs dacite showing narrow, calcium silicate (skarn type), diopside-rich, reaction rim, R.

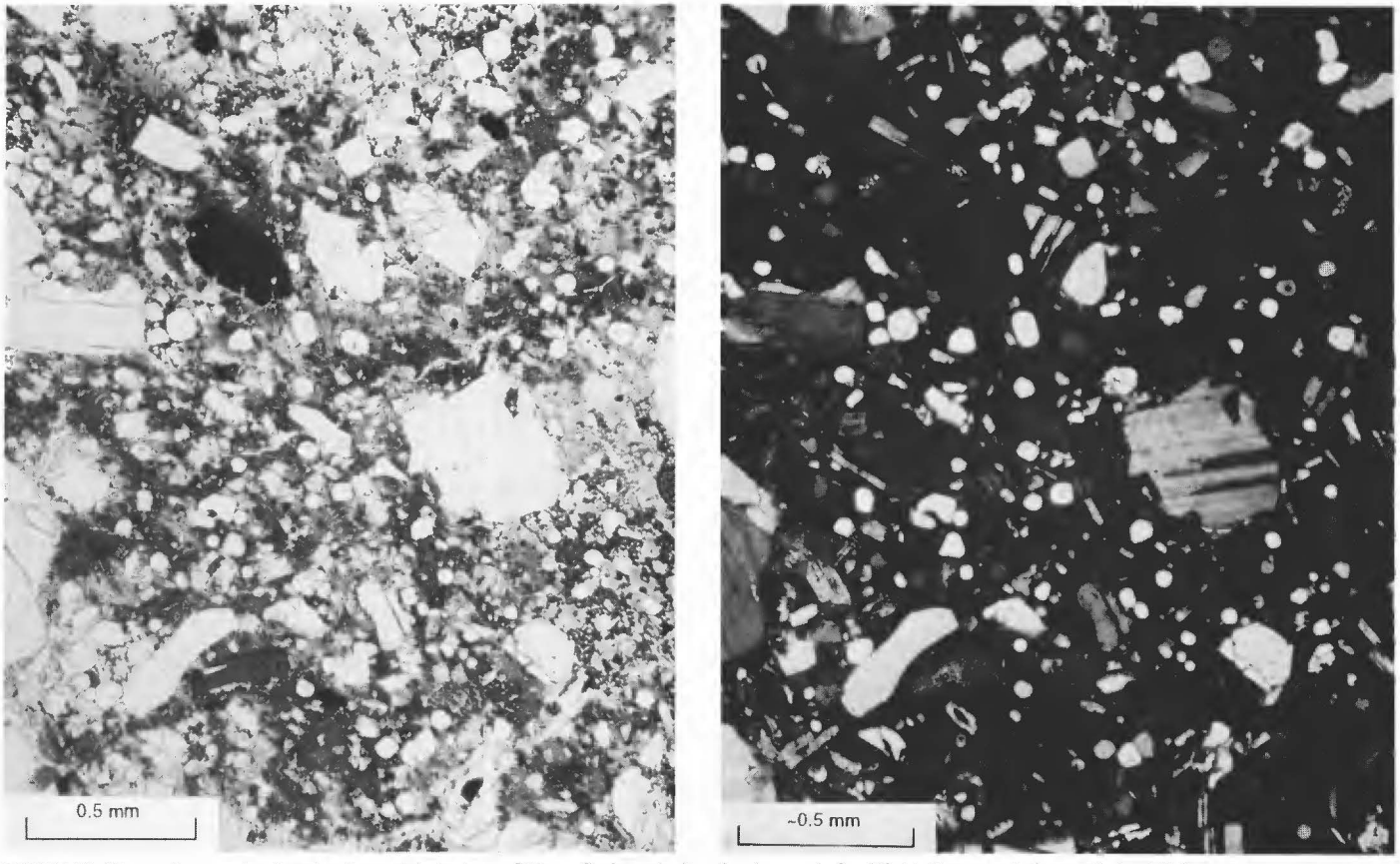


FIGURE 13. Photomicrographs showing the matrix texture of Horse Springs dacite. A, plane polarized light. B, crossed plane polarized light.

TABLE 2. Chemical and modal analyses of Horse Springs dacite, cognate quartz monzonite inclusions, and Blue Canyon Tuff. Analysts: Sample numbers 1,2,3,5 and 7 major oxides by J. Baker, A. Bartel, D. Siems, J. Taggart, J. Wahlberg; trace elements by D. Fey, R. Yeoman and D. Bove. Sample number 4 from D.P. Jones, 1980. Sample number 6 by Bornhorst, 1980. (-) indicates not analyzed or not found.

Sample No.	1	2	3	4	5	6	7
Field No.	P-5-78	BP-1-88	BP-2-88	J-218	BP-6A-85	T-377	HW-1B-82
			MAJOR OXIDES				
			(weight percent, recalculated water-free)				
SiO_2	66.6	67.5	66.4	65.6	67.6	67.8	70.27
Al_2O_3	15.6	15.7	15.7	16.3	15.6	15.7	15.15
Fe_2O_3	3.86*	4.56*	4.64*	3.66	2.86*	3.02	0.90
MgO	1.32	1.03	1.07	1.25	1.34	1.42	0.52
CaO	3.53	2.31	3.12	3.98	3.54	3.17	1.43
Na_2O	3.51	3.16	3.60	3.89	4.19	3.34	2.90
K_2O	4.55	4.70	4.37	4.14	3.94	4.25	7.05
TiO_2	0.62	0.68	0.67	0.59	0.58	0.53	0.44
P_2O_5	0.33	0.23	0.30	0.23	0.21	0.18	0.08
MnO	0.11	0.07	0.11	0.07	0.04	0.04	0.05
FeO	—	—	—	—	—	0.19	1.21
Total	100.03	99.94	99.98	99.71	99.90	99.64	100.00
*Total iron as Fe_2O_3							
			TRACE ELEMENTS				
			(parts per million; L, indicates detected at limit shown)				
Ba	—	898	1002	—	860	969	—
Cr	—	—	—	—	9	25	—
Cu	—	78L	78L	—	11	18	—
Ga	—	16L	20	—	17	<20	—
Ni	—	—	—	—	8	19	—
Rb	—	145	119	—	—	114	—
Sr	—	384	514	—	520	481	—
Th	—	18L	18L	—	17	19.4	—
V	—	—	—	—	45	41	—
Y	—	32	28	—	22	30	—
Zn	—	79	71	—	35	134	—
Zr	—	247	215	—	—	245	—
			MODES				
			(volume percent)				
Groundmass	72	72	71	65.2	61	61.9	83.3
Sanidine	Trace	Trace	Trace	2.0	Trace	—	4.7
Quartz	—	Trace	Trace	0.2	—	0.3	—
Sodic plagioclase	21	24.3	22.6	25.8	30	28.9	10.7
Biotite	3.5	1.4	2.0	2.7	3.5	5.1	0.5
Clinopyroxene	3	1.1	2.7	2.2	3	2.2	Trace
Hornblende	—	—	—	—	1	—	—
Opaque oxide	0.5	0.5	1.5	1.9	1.5	1.5	0.7
Zircon	—	—	Trace	Trace	Trace	—	—
Apatite	Trace	—	Trace	—	Trace	—	—
Total	100	99.3	99.8	100	100	99.9	99.9

Sample descriptions

1. Pumice block from roadcut on north side of NM-12 west of Old Horse Springs in Bell Peak Quadrangle.
2. Pumice block from outcrops on west side of Cerro Caballo ridge south of NM-12 (elevation about 7260 ft) in Bell Peak Quadrangle.
3. Pumice block from outcrops on west side of Cerro Caballo ridge south of NM-12 (elevation about 7420 ft) in Bell Peak Quadrangle.
4. Horse Springs dacite matrix from outcrops on east side of White Rock Canyon at White Rock Spring in Wallace Mesa Quadrangle. From D.P. Jones, 1980.
5. Cognate quartz monzonite inclusion from outcrops on west side of Cerro Caballo ridge (elevation about 7500 ft) in Bell Peak Quadrangle.
6. Cognate quartz monzonite inclusion from outcrops on west side of Cerro Caballo ridge south of NM-12 in Bell Peak Quadrangle. Collected and analyzed by T.J. Bornhorst (1980, p. 593).
7. Blue Canyon Tuff from roadcut on north side of NM-12 near west edge of Horse Mountain West Quadrangle.



FIGURE 14. Photomicrograph showing quartz and alkali feldspar (twinned) in granophyric groundmass of cognate quartz monzonite inclusions in Horse Springs dacite. Phenocrysts in view are augitic pyroxene and plagioclase. Crossed plane polarized light.

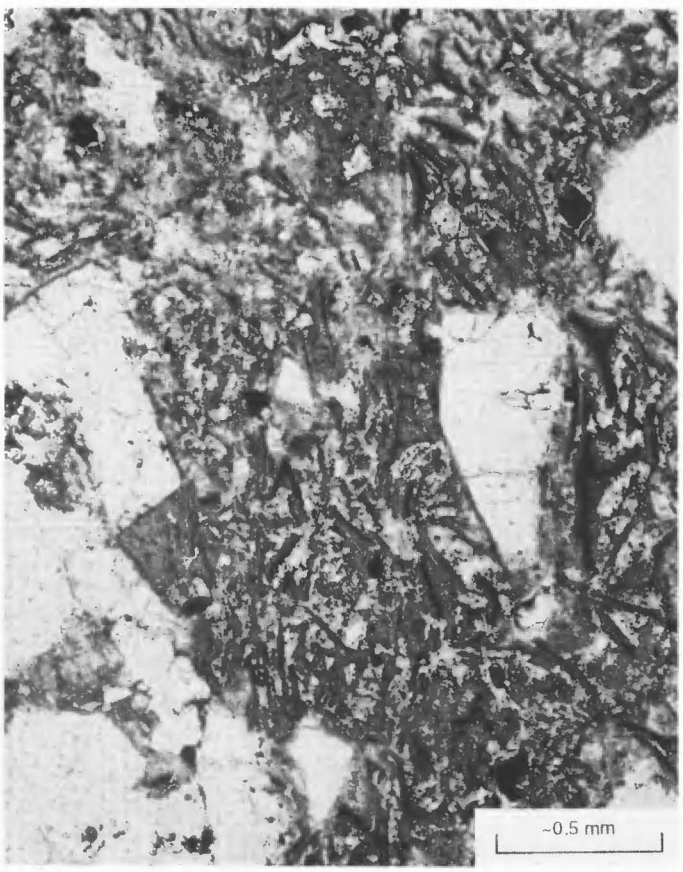


FIGURE 15. Photomicrograph of Blue Canyon Tuff showing vitroclastic matrix of devitrified glass shards between plagioclase phenocrysts. Crossed plane polarized light.

grained outer zones (colored by a fine magnesioferrite dust) and cores of coarsely crystalline quartz, hematite and calcite. Forsteritic olivine occurs as inclusions in hematite crystals; it contains approximately 1.8% total iron (Table 3). The bright-red cathodoluminescence of the forsterite suggests that all of the iron is in the ferric state. This assemblage of ferric-iron minerals indicates a high oxygen fugacity during formation, which may have involved recrystallization of preexisting iron oxides. Although no magnetite has been observed in the nodules, which contain only ferric-iron and Mn3+ phases (Table 4), textural evidence, mainly fine-grained aggregates of iron oxide that have pseudomorphic outlines, indicates probable replacement of pre-existing iron-oxide crystals.

Zinc in the jasperoid inclusions seems to be dominantly in the magnesioferrite (0.33-2.93 wgt % ZnO; Table 5). Zinc is also present in aluminum spinels (1-27 wgt %; Table 5), but the spinels are a very minor phase volumetrically. The zinc-bearing phases may have been produced by recrystallization and oxidation during thermal metamorphism of earlier-formed oxides, such as magnetite and franklinite, or by desulfidization of sphalerite. Zinc and other trace metals in the mineralized jasperoid inclusions are shown in Table 6, where zinc is seen to be as much as 1% (10,000 ppm) of some inclusions.

Reaction zones between the jasperoid inclusions and the enclosing dacite pumice breccia have a largely different mineral assemblage than the inclusions themselves (Fig. 18). Calc-silicate skarn consists of greenish-yellow, diopside-rich border zones, a few centimeters thick, around many of the in-situ jasperoid nodules. Euhedral diopside crystals are commonly zoned, and FeO ranges between 4 and 15% (Table 7). Diopside in the skarn reaction zones may be accompanied by green to brown, euhedral andradite garnet that ranges in composition from about andradite$_{90}$—grossular$_{8}$ to andradite$_{34}$—grossular$_{34}$ (Table 7). Other minerals found in the reaction zone include light-pink montmorillonite clay and phlogopite mica (Table 4). Within the tuff adjacent to the reaction zone, plagioclase phenocrysts are altered to a fine-grained mixture of clays, micas, and other unidentified K and Mg silicates.

Diopside also occurs as free-growing, transparent, yellowish-green prisms, a few tenths of a millimeter long, in vugs and fractures in the jasperoid inclusions and in miarolitic cavities in the cognate quartz monzonite blocks, where it commonly is accompanied by hematite and prismatic to bladed pseudobrookite ($Fe^{+3}{}_2TiO_5$; Table 5). Titanite coats some pseudobrookite crystals.

ORIGIN AND SIGNIFICANCE OF MINERALIZED INCLUSIONS

Two main problems concerning the formation of the mineralized inclusions are (1) place of origin and physical-chemical environment of jasperoid development and associated mineralization; and (2) place of origin and physical-chemical environment of calc-silicate reaction zones on the margins of jasperoid inclusions. There are two alternative explanations: (1) both mineralized jasperoid and calc-silicate reaction zones formed in the same place as parts of a single alteration process; or (2) the mineralized jasperoid and the reaction zones formed in separate places as a result of different processes.

Some of the considerations in evaluating these alternatives are:

1. The delicate, granular, calc-silicate reaction zones around jasperoid inclusions are essentially unbroken where inclusions are found in place, but are almost never found attached to the inclusions in float, attesting to their vulnerability during transport.

2. The mineral assemblage in the calc-silicate zones consists of variable proportions of diopside, garnet, phlogopite and clay minerals. Except for the clays, this assemblage is consistent with the

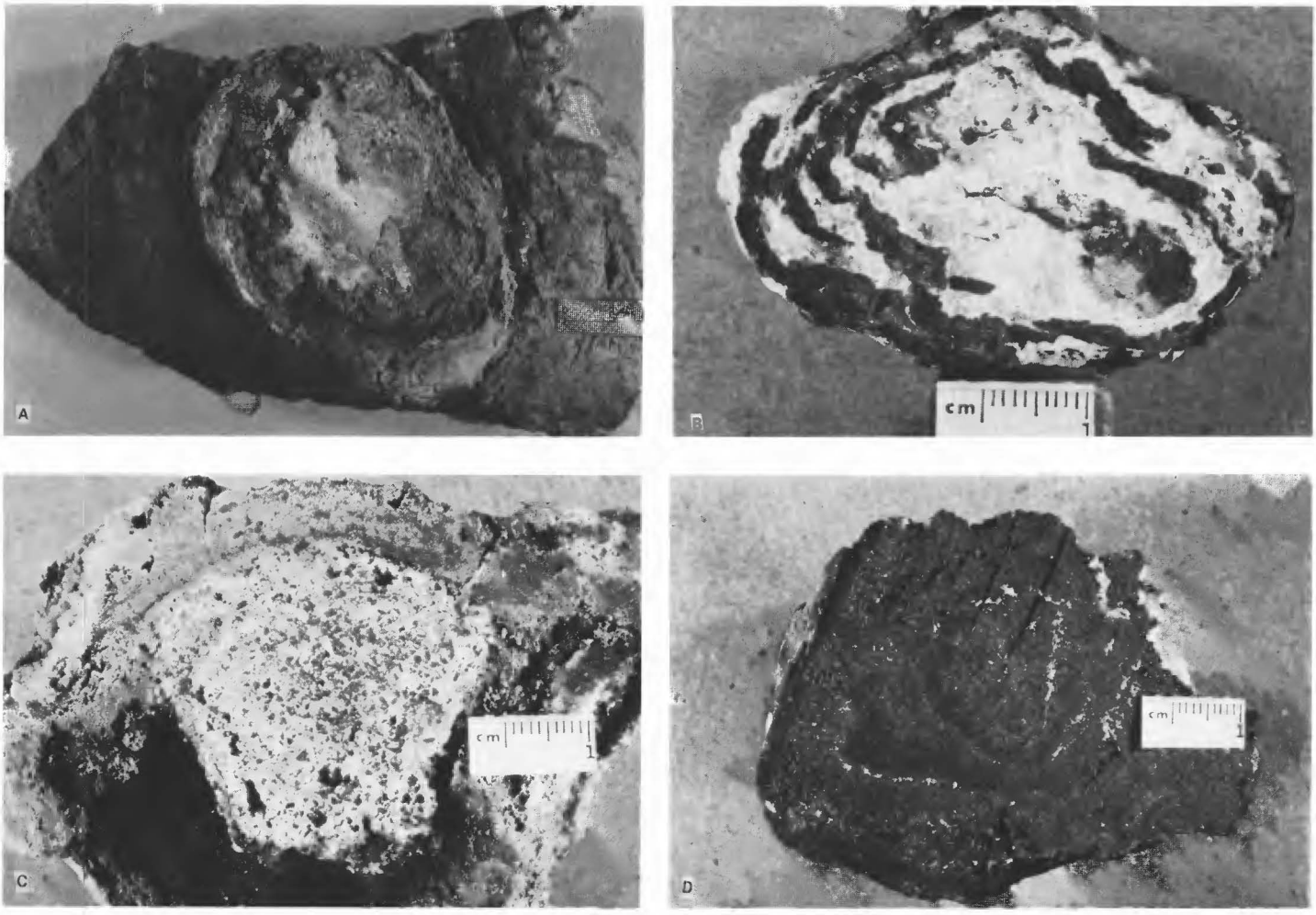


FIGURE 16. Accidental inclusions of mineralized jasperoid in Horse Springs dacite showing different form and composition. A, Jasperoid inclusion showing core of quartz, hematite and calcite surrounded by jasperoid containing fine-grained magnesioferrite. B, Jasperoid inclusion showing concentric layers of quartz and calcite and iron oxides. C, Jasperoid inclusion showing core of calcite, quartz, hematite and magnesioferrite surrounded by a red outer layer of quartz, hematite and magnesioferrite. D, Iron oxide-rich jasperoid inclusion containing disseminated hematite, magnesioferrite and quartz.

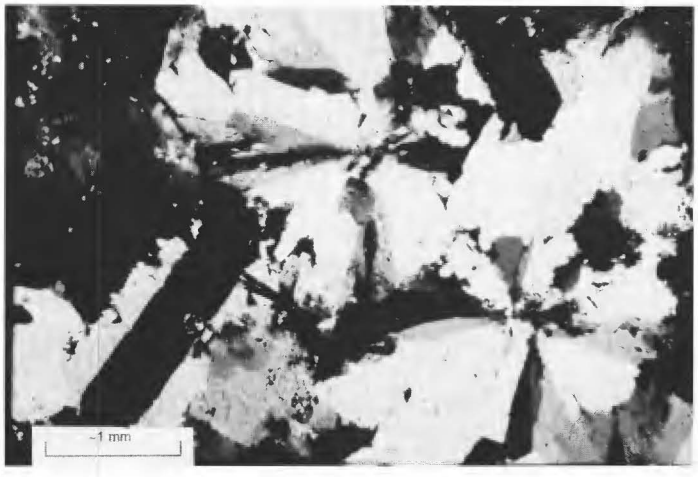


FIGURE 17. Photomicrograph showing spherulitic quartz and coarse, platy hematite crystals in jasperoid inclusion. Crossed plane polarized light.

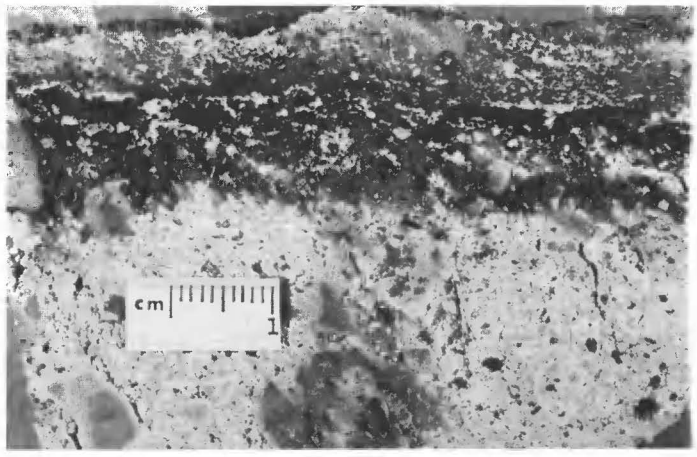


FIGURE 18. Cross section of calc-silicate reaction skarn surrounding jasperoid inclusion from inside of reaction zone (top) into enclosing dacite breccia (bottom), showing: (1) 1 mm red layer of hematite and phlogopite; (2) 4-9 mm pale-green exoskarn layer of granular diopside and montmorillonite, and minor hematite and feldspar; (3) 6-11 mm dark-green endoskarn layer of diopside, minor hematite, and variably altered feldspar; (4) dacite breccia host rock showing scattered development of diopside and clay, and plagioclase phenocrysts with altered borders.

TABLE 3. Microprobe analyses of mineral phases in jasperoid, calc-silicate skarn reaction rims, and altered Horse Springs dacite. Analyses on ARL-SEMQ microprobe, 20 sec. counting times, MAGIC-IV matrix correction program. Analysis of olivine and calcite, 10 kV accelerating voltage, 5 nA sample current; standards: K,Al,Si, orthoclase; Mg, dolomite; Ca, calcite; Mn, rhodochrosite; Fe, siderite. Analysis of mica and feldspar, 15 kV accelerating voltage, 10 nA sample current; standards: Na, albite; K, orthoclase; Mg, diopside; Ca,Al,Si, grossular; Mn,Fe, spessartine-almandine; Ti, titanite; Cr, chromite; Zn, willemite. (-) indicates not analyzed.

	Phl-1	For-1	Cc-1	Pla-1	Alt-1	Alt-2
			(weight percent)			
Na_2O	0.57	—	—	7.54	—	0.29
K_2O	9.80	—	—	1.04	8.14	0.15
MgO	28.15	59.08	0.03	0.02	0.21	9.48
CaO	0.14	0.02	53.82	5.25	6.32	1.24
SrO	—	—	0.02	—	0.00	—
MnO	0.00	0.08	0.00	0.02	0.00	0.00
FeO	0.59	1.82	0.00	0.24	0.21	0.81
ZnO	0.07	0.03	—	0.01	—	0.02
Al_2O_3	10.03	0.01	0.08	22.07	25.12	16.87
Cr_2O_3	0.00	—	—	0.00	—	—
SiO_2	44.26	39.11	0.00	61.80	59.37	56.65
TiO_2	0.14	0.04	—	0.00	—	0.01
CO_2	—	—	42.28*	—	—	—
Total	93.75	100.19	96.23	98.01	99.37	85.52
			(cation proportions)			
Na	0.078	—	—	0.663	—	0.039
K	0.882	—	—	0.060	0.650	0.013
Mg	2.961	2.087	0.001	0.001	0.020	0.974
Ca	0.011	0.001	0.997	0.255	0.424	0.092
Sr	—	—	0.000	—	0.000	—
Mn^{+2}	0.000	0.002	0.000	0.001	0.000	—
Fe^{+2}	0.035	0.036	0.000	0.009	0.011	0.047
Zn	0.004	0.001	—	—	—	—
Al	0.834	—	0.002	1.179	1.855	1.370
Si	3.122	0.927	0.000	2.802	3.719	3.904
Ti	0.007	0.001	—	0.000	—	—
Σox.	11.000	4.000	1.001	8.000	11.000	11.000

Sample descriptions

Phl-1 = phlogopite mica at contact of jasperoid nodule BP-46-86 with skarn rim.
For-1 = olivine inclusion in hematite, within jasperoid nodule BP-6B-85.
Cc-1 = calcite intergrown with quartz in jasperoid nodule BP-6G-85.
Pla-1 = unaltered core (sodic andesine) of plagioclase phenocryst in tuff, within outer part of calc-silicate reaction rind around nodule BP-46-86.
Alt-1 = altered rim of plagioclase phenocryst (mineral composition unknown).
Alt-2 = Mg-Al-silicate (mineral identity unknown) surrounding an altered plagioclase phenocryst.
*calculated amount of CO_2 in calcite.

TABLE 4. List of minerals in the jasperoid inclusions, calc-silicate skarn reaction rims, and altered Horse Springs dacite.

Hematite
Magnesioferrite
Spinel (zincian)
Franklinite/gahnite
Pseudobrookite
Sphene
Forsterite
Diopside
Andradite
Phlogopite
Montmorillonite
Quartz
Calcite

pyroxene-hornfels facies of contact metamorphism, indicating a formation temperature between about 550° and 700°C. The intensity of alteration around the jasperoid decreases outward into the pumice breccia.

3. The mineral assemblage in the jasperoid, mainly quartz, calcite and hematite, is typical of low-temperature metasomatism. However, magnesioferrite and tiny forsterite inclusions in the hematite indicate a higher temperature of formation.

4. The pumice breccia deposit is not welded.

5. Unaltered limestone xenoliths have not been observed.

6. The ancient fumaroles lack evidence of iron or other sublimates deposited during degassing of the pumice breccia.

7. The anomalous abundance of several metals, notably iron, zinc and manganese,and in lesser amounts copper, vanadium, nickel and lead, is evidence of some type of active mineralizing process.

8. Quartz replacement textures observed are typically low-temperature jasperoidization.

9. Iron-oxide replacement textures in the jasperoid nodules suggest replacement by magnesioferrite of pre-existing, probably lower temperature, iron oxides.

TABLE 5. Microprobe analyses of oxide minerals in jasperoid inclusions. Analyses on ARL-SEMQ microprobe, 15 kV accelerating voltage, 15 nA sample current, 20 sec. counting times, MAGIC-IV matrix correction program. Standards for analysis of oxide minerals: Mg,Al, spinel; Ca,Ti,Si, titanite; Fe, hematite; Mn, spessartine; Zn, willemite.

	Hem-1	Hem-2	Hem-3	Mgf-1	Mgf-2	Mgf-3	Spn-1	Spn-2	Spn-3
					(weight percent)				
MgO	0.22	0.35	0.16	21.71	21.62	20.72	27.11	10.39	5.59
CaO	0.01	0.00	0.00	0.01	0.92	0.18	0.06	0.03	1.25
MnO	0.04	0.74	0.17	1.22	3.32	3.85	0.25	10.61	10.91
ZnO	0.01	0.00	0.00	0.33	0.47	2.93	1.05	11.10	27.46
Fe_2O_3	98.29	99.10	100.39	79.22	68.14	72.52	16.61	30.28	34.49
Al_2O_3	0.23	0.08	1.03	0.29	5.37	0.98	53.97	11.87	8.95
SiO_2	0.01	0.01	0.07	0.02	0.01	0.22	0.22	0.13	0.16
TiO_2	0.14	0.04	0.02	0.00	0.00	0.04	0.00	0.04	0.06
Total	98.95	100.32	101.84	102.80	99.85	101.44	99.27	96.79	88.87
					(cation proportions)				
Mg	0.009	0.014	0.006	1.037	1.029	1.002	1.029	0.537	0.329
Ca	—	—	—	—	0.032	0.001	0.002	0.001	0.053
Mn^{+3}	0.001	0.015	0.003	0.033	0.090	0.106	0.005	0.312	0.365
Zn	—	—	—	0.008	0.011	0.070	0.020	0.284	0.802
Fe^{+3}	1.981	1.973	1.958	1.910	1.637	1.770	0.318	1.374	1.026
Al	0.007	0.003	0.032	0.011	0.202	0.038	1.620	0.485	0.417
Si	—	—	0.002	0.001	—	0.007	0.006	0.004	0.006
Ti	0.003	—	—	—	—	0.001	—	0.001	0.002
Oxygen atoms	2.999	3.000	3.000	3.978	3.966	3.960	3.978	4.088	3.912

Sample descriptions

Hem-1 = coarse hematite in jasperoid nodule BP-6G-85.
Hem-2 = coarse hematite in jasperoid nodule BP-6C-85.
Hem-3 = coarse hematite, host for olivine inclusions in jasperoid BP-6B-85.
Mgf-1 = magnesioferrite, intergrown with hematite in jasperoid BP-6A-85.
Mgf-2 = magnesioferrite crystal (about 20 microns) in jasperoid BP-6G-85.
Mgf-3 = fine-grained magnesioferrite in jasperoid BP-6A-85.
Spn-1 = yellowish-brown spinel crystal in jasperoid BP-6B-85.
Spn-2 = fine-grained spinel (complex solid solution) in jasperoid BP-6E-85.
Spn-3 = very fine-grained spinel (franklinite/gahnite) in jasperoid BP-6G-85.

TABLE 6. Atomic absorption (AA) and semiquantitative spectrographic analyses (6-step D-C arc method) of mineralized jasperoid inclusions. G, greater than value shown; N( ), not detected at level of value shown; L( ), detected, but less than value shown. Analysts: D.E. Detra, R.T. Fairfield, L.S. Landon and C.D. Taylor.

	AA		Percent				Parts per million										
Field No.	Au	Ag	Fe	Mg	Ca	Ti	Mn	B	Ba	Be	Co	Cu	Ni	Pb	Sn	V	Zn
BP-2-85	N(0.05)	N(0.05)	G20	1	L(0.05)	0.15	300	30	200	N(1)	70	100	100	N(10)	N(10)	300	2000
BP-3-85	N	N	2	3	5	0.15	200	30	N(20)	2	10	15	15	N	N	15	N(200)
BP-6A-85	N	N	3	1	1.5	0.3	500	10	700	1.5	15	10	7	15	N	70	N
BP-6B-85	N	N	20	1	0.2	0.03	2000	15	20	L(1)	70	100	100	10	20	150	7000
BP-6D-85	N	N	15	2	2	0.02	3000	20	50	N	50	300	30	70	15	70	10000
BP-6E-85	N	N	G20	1	0.7	0.03	2000	10	20	N	70	50	100	N	15	300	1000
BP-6F-85	N	N	20	1	2	0.015	1500	10	20	N	50	100	70	50	N	100	5000

TABLE 7. Microprobe analyses of diopside and garnet in calc-silicate skarn reaction rims. Analyses on ARL-SEMQ microprobe, 20 sec. counting times, MAGIC-IV matrix correction program. Analyses of pyroxenes Di-1 to Di-4, 10 kV accelerating voltage, 5 nA sample current; standards: K,Al,Si, orthoclase; Mg, dolomite; Ca, calcite; Mn, rhodochrosite; Fe, siderite. Analyses Di-5 and of garnet, 15 kV accelerating voltage, 10 nA sample current; standards: Na, albite; K, orthoclase; Mg, diopside; Ca,Al,Si, grossular; Mn,Fe, spessartine-almandine; Ti, titanite; Cr, chromite; Zn, willemite. Dash (-) indicates not analyzed.

	Di-1	Di-2	Di-3	Di-4	Di-5	And-1	And-2	And-3	And-4
					(weight percent)				
Na_2O	—	—	—	—	0.35	0.00	0.01	0.01	0.02
K_2O	0.02	0.03	0.02	0.00	0.00	0.00	0.00	0.01	0.01
MgO	17.52	13.29	15.03	13.71	9.40	0.19	0.20	0.17	0.18
CaO	25.19	24.96	23.18	24.37	22.78	32.52	32.84	33.24	33.11
SrO	0.00	0.06	0.02	0.01	—	—	—	—	—
MnO	0.05	0.14	0.76	0.04	0.13	0.09	0.11	0.10	0.12
FeO	4.06	6.34	9.00	10.58	14.75	28.44*	27.09*	24.78*	20.38*
ZnO	—	—	—	—	0.03	0.00	0.00	0.00	0.03
Al_2O_3	2.95	5.43	0.64	3.58	2.17	1.73	2.58	4.41	7.20
Cr_2O_3	—	—	—	—	0.00	0.01	0.00	0.00	0.02
SiO_2	53.57	51.16	53.85	50.48	48.90	35.78	35.58	36.27	37.14
TiO_2	—	—	—	—	0.12	0.24	0.42	0.07	0.13
Total	103.36	101.41	102.50	102.77	98.63	99.00	98.83	99.06	98.34
					(cation proportions)				
Na	—	—	—	—	0.027	0.000	0.001	0.002	0.003
K	0.001	0.001	0.001	0.000	0.000	0.000	0.000	0.001	0.001
Mg	0.928	0.725	0.818	0.754	0.549	0.024	0.025	0.021	0.022
Ca	0.959	0.979	0.907	0.963	0.957	2.938	2.975	2.960	2.913
Sr	0.000	0.001	0.000	0.000	—	—	—	—	—
Mn	0.002	0.004	0.024	0.001	0.004	0.007	0.008	0.007	0.008
Fe	0.121	0.194	0.275	0.326	0.484	1.805	1.724	1.550	1.259
Zn	—	—	—	—	0.001	0.000	0.000	0.000	0.002
Al	0.123	0.234	0.028	0.156	0.100	0.172	0.257	0.432	0.697
Cr	—	—	—	—	0.000	0.001	0.000	0.000	0.002
Si	1.903	1.872	1.967	1.861	1.917	3.017	2.983	3.015	3.050
Ti	—	—	—	—	0.004	0.015	0.027	0.004	0.008
Σox.	6.001	5.999	6.000	6.000	6.000	12	12	12	12

Sample descriptions

Di-1 = unzoned diopside crystal in calc-silicate rind on nodule BP-46-86.
Di-2 = diopside crystal in calc-silicate rind on nodule BP-6F-85.
Di-3 = colorless core of diopside crystal in rind on BP-46-86.
Di-4 = yellowish-green rim of diopside crystal in rind on BP-46-86.
Di-5 = brown zone in a diopside crystal in rind on BP-46-86.
And-1 = core of andradite garnet crystal in calc-silicate rind, BP-6-86.
And-2 = rim of same garnet crystal.
And-3 = garnet crystal in calc-silicate rind, BP-6-86.
And-4 = garnet crystal in calc-silicate rind, BP-6-86.
*iron in garnet analysis is expressed as Fe_2O_3.

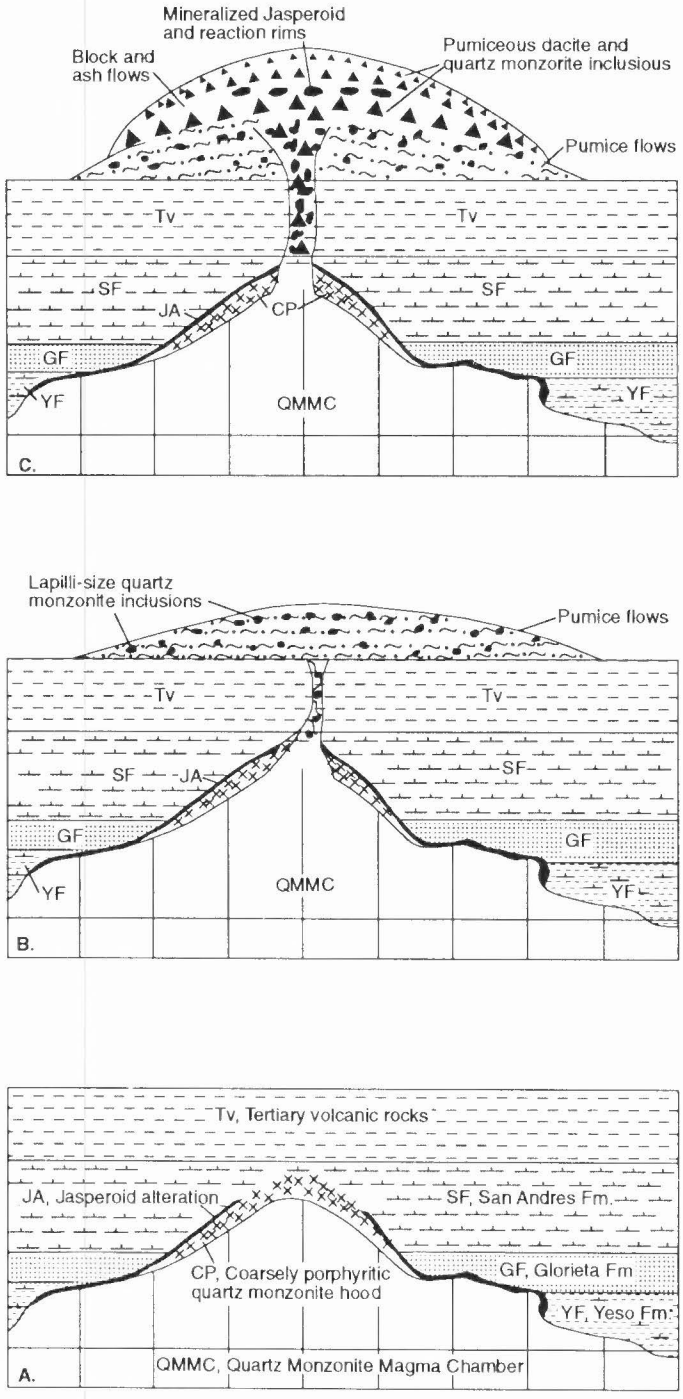


FIGURE 19. Diagrams showing the evolution of the Horse Springs dacite and the origin of the mineralized jasperoid accidental inclusions. A, Pre-eruption phase; B, Early eruptive phase, pumice flows; C, Late eruptive phase.

10. The apparent concentration of mineralized jasperoid xenoliths in the upper part of the zone in which the quartz monzonite blocks are largest and most concentrated suggests an eruptive stratigraphy progressing from the eruption of cognate quartz monzonite to jasperoidized wall rocks.

CONCLUSIONS

The observed field relationships, mineral phases, and textures suggest the following sequence of events in the evolution and eruption of the Horse Springs dacite and its inclusions:

1. Jasperoidization and iron and zinc mineralization of pre-Tertiary wall rocks and formation of iron oxides by hydrothermal solutions at the top of a dacitic magma chamber preceded eruption of the dacite pumice breccia (Fig. 19). Crystallization of the coarse-grained quartz monzonite may have occurred in the roof zone of the magma chamber at this time.

2. Volatile pressure in the magma chamber eventually exceeded the confining pressure and initiated eruption of pyroclastic pumice flows, which contain small accidental inclusions of quartz monzonite but no pre-Tertiary inclusions.

3. After the premonitory eruptions, continued volatiles exsolution increased the pressure in the magma chamber to the point that a massive failure of the chamber roof led to eruption of the block-and-ash flows and the entrainment of abundant shattered quartz monzonite roof rocks and lesser amounts of jasperoidized and mineralized pre-Tertiary wall-rock. Similarities in composition between pumiceous dacite blocks and more massive, but vesicular to miarolitic, quartz monzonite inclusions suggest gradation in the roof of the magma chamber between pumiceous dacite and porphyritic quartz monzonite.

4. During cooling of the dacite pumice breccia, reaction between the mineralized jasperoid xenoliths and the hot pumice breccia produced the diopside-rich skarn zones. Original magnetite and (or) other iron oxides in the jasperoid xenoliths may have been recrystallized to the ferric phases hematite, magnesioferrite and ferric-iron-rich forsterite at this time. Diopside and pseudobrookite, found in miarolitic cavities in the quartz monzonite, may also have formed then (according to Lindsley, 1965, pseudobrookite is unstable below 585°C). Montmorillonite clay, phlogopite and other minerals were formed by alteration of the pumice breccia at lower temperatures, as cooling of the pumice breccia proceeded.

A low to moderate potential for undiscovered resources of base and ferrous metals, particularly zinc and iron, and possibly associated silver and gold, is indicated by the anomalous metals (Table 7) in the mineralized jasperoid inclusions (Ratté et al., 1988). The most likely type of deposit might be a contact-metasomatic deposit accompanied by replacement and vein deposits related to intrusion of a silicic pluton into pre-Tertiary sedimentary rocks at shallow depths. Pre-Tertiary rocks may be within a few hundred meters of the surface in the vicinity of the probable source vent of the pumice breccia of Old Horse Springs, as indicated by outcrops of pre-Tertiary sedimentary rocks about 10 km northeast of the proposed vent. The zinc-rich middle Tertiary ore deposits in pre-Tertiary limestones in the Magdalena district, about 100 km east of the Horse Springs area, provide a possible model for the type of deposit that could be present beneath the surface here.

REFERENCES

Bornhorst, T.J., 1976, Volcanic geology of the Crosby Mountains and vicinity, Catron County, New Mexico [M.S. thesis]: Albuquerque, University of New Mexico, 113 p.

Bornhorst, T.J., 1980, Major and trace element geochemistry and mineralogy of upper Eocene to Quaternary volcanic rocks of the Mogollon-Datil volcanic field, southwestern New Mexico [Ph.D. dissertation]: Albuquerque, University of New Mexico, 1108 p.

Bornhorst, T.J. and Elston, W.E., 1978, Supplemental roadlog no. 8, Reserve to Magdalena via Horse Springs and Datil: New Mexico Geological Society, Special Publication 7, p. 99-106.

Cather, S.M., 1986, Volcano-sedimentary evolution and tectonic implications of the Datil Group (latest Eocene-early Oligocene), west-central New Mexico [Ph.D. dissertation]: Austin, University of Texas, 484 p.

Cather, S.M., McIntosh, W.C. and Chapin, C.E., 1987, Stratigraphy, age, and rates of deposition to the Datil Group (upper Eocene-lower Oligocene), west-central New Mexico: New Mexico Geology, v. 9, p. 50-54.

Elston, W.E., 1984, Mid-Tertiary ash flow tuff cauldrons, S.W. New Mexico: Journal of Geophysical Research, v. 89, no. B-10, p. 8733-8750.

Fisher, R.V. and Schminke, H.-U., 1984, Pyroclastic rocks: Springer-Verlag, 472 p.

Jones, D.P., 1980, Volcanic geology of the Alegres Mountain area, Catron County, New Mexico [M.S. thesis]: Albuquerque, University of New Mexico, 76 p.

Lindsley, D.H., 1965, Iron-titanium oxides: Carnegie Institute of Washington, 1964 Yearbook, p. 144-148.

Marvin, R.F., Naeser, C.W., Bikerman, M., Mehnert, H.H. and Ratté, J.C., 1987, Isotopic ages of post-Paleocene igneous rocks within and bordering the Clifton 1x2 degree quadrangle, Arizona-New Mexico: New Mexico Bureau of Mines and Mineral Resources, Bulletin 118, 50 p.

Osburn, G.R. and Chapin, C.E., 1983, Nomenclature for Cenozoic rocks of northeast Mogollon-Datil volcanic field, New Mexico: New Mexico Bureau of Mines and Mineral Resources, Stratigraphic Chart 1.

Ratté, J.C. and Modreski, P.J., 1989, Selected volcanic features of the western Mogollon-Datil volcanic field; New Mexico Bureau of Mines and Mineral Resources, Memoir 46, p. 68-80.

Ratté, J.C., McIntosh, W.C. and Houser, B.B., 1991, Geologic map of the Horse Mountain West quadrangle, Catron County, New Mexico: U.S. Geological Survey, Geologic Quadrangle Map GQ-1685, scale 1:24,000.

Ratté, J.C., Saltus, R. and Turner, R.L., 1988, Mineral resources of the Horse Mountain and Continental Divide Wilderness Study Areas, Catron County, New Mexico: U.S. Geological Survey, Bulletin 1734, 16 p.

Smith, R.L., 1960, Zones and zonal variations in welded ash flows: U.S. Geological Survey, Professional Paper 354-F, p. 149-159.

Stearns, C.E., 1962, Geology of the north half of the Pelona quadrangle, Catron County, New Mexico: New Mexico Bureau of Mines and Mineral Resources, Bulletin 78, p. 46.



Plains of San Agustin from southeast base of Horse Mountain, New Mexico. View is S22°E. Shaw Mountain on horizon, to right of center, consists of Bearwallow Mountain Andesite overlying Oligocene ignimbrites of the Mogollon Group. Unnamed hills left of center show wave-cut cliffs just above the plains. These cliffs are cut in thin ignimbrites of the Datil and Mogollon groups. Camera station is alongside Highway 12 in SE ¼ sec. 16, T4S, R12W. Altitude is about 2140 m. Wayne Lambert photograph No. 93L75. August 15, 1993, 12:14 p.m. MDT.